J Neuropathol Exp Neurol
Vol. 78, No. 4, April 2019, pp. 348–364
doi: 10.1093/jnen/nlz008

ORIGINAL ARTICLE

Axotomy Induces Phasic Alterations in Luman/CREB3 Expression and Nuclear Localization in Injured and Contralateral Uninjured Sensory Neurons: Correlation With Intrinsic Axon Growth Capacity

Jovan C.D. Hasmatali, MD, PhD, Jolly De Guzman, MD, Ruiling Zhai, MD, Lisa Yang, MD, Nikki A. McLean, PhD, Catherine Hutchinson, MSc, Jayne M. Johnston, RT, Vikram Misra, PhD, and Valerie M.K. Verge, PhD

Abstract

Luman/CREB3 is an important early retrograde axotomy signal regulating acute axon outgrowth in sensory neurons through the adaptive unfolded protein response. As the injury response is transcriptionally multiphasic, a spatiotemporal analysis of Luman/CREB3 localization in rat dorsal root ganglion (DRG) with unilateral L4–L6 spinal nerve injury was conducted to determine if Luman/CREB3 expression was similarly regulated. Biphasic alterations in Luman/CREB3 immunofluorescence and nuclear localization occurred in neurons ipsilateral to 1-hour, 1-day, 2-day, 4-day, and 1-week injury, with a largely parallel, but less avid response contralaterally. This biphasic response was not observed at the transcript level. To assess whether changes in neuronal Luman expression corresponded with an altered intrinsic capacity to grow an axon/neurite in vitro, injury-conditioned and contralateral uninjured DRG neurons underwent a 24-hour axon growth assay. Two-day injury-conditioned neurons exhibited maximal outgrowth capacity relative to naïve, declining at later injury-conditioned timepoints. Only neurons contralateral to 1-week injury exhibited significantly higher axon growth capacity than naïve. In conclusion, alterations in neuronal injury-associated Luman/CREB3 expression support that a multiphasic cell body response occurs and reveal a novel contralateral plasticity in axon growth capacity at 1-week post-injury. These adaptive responses have the potential to inform when repair or therapeutic intervention may be most effective.

Key Words: Axotomy, Contralateral, LZIP, Peripheral nerve injury, Unfolded protein response.

INTRODUCTION

A characteristic of peripheral nervous system (PNS) neurons is their capacity for regeneration and self-repair. Axotomy alters neuronal phenotype as the priority changes from signal transmission to axon regeneration. This requires abundant lipid and protein synthesis (1–3), originating from somal or axoplasmic endoplasmic reticuli (ER) (4). The augmented protein production and vesicular trafficking during regeneration can result in elevated levels of unfolded or misfolded proteins, with ER stress ensuing (5). Adaptive cellular mechanisms such as the unfolded protein response (UPR) can ameliorate this stress state, re-establish ER homeostasis and aid in the regeneration of axons (6–8). Conversely, maladaptive ER stress is increasingly linked to neurologic disease, neuronal loss, neuropathic pain, and impaired regeneration (9–11).

There is a paucity of information about the transcriptional regulators of the ER stress/UPR associated with nerve injury. However, we have recently identified an important regulator of this pathway, Luman/CREB3 (also known as LZIP; herein called Luman). Luman, through its regulation of the UPR and cholesterol biosynthesis, plays a crucial role in the ability of a sensory neuron to regrow an axon early after injury (7, 12). Luman is a member of the CREB/ATF family (13) and the first known cellular ligand for host cell factor-1 (14). While initially recognized for its role in viral latency and reactivation (13–16), its localization to the ER membrane and links to the UPR suggested additional roles. Luman protein

From the Department of Anatomy, Physiology and Pharmacology (JCDH, JDG, RZ, NAM, CH, JMJ, VMKV); Cameco MS Neuroscience Research Center (JCDH, JDG, RZ, LY, NAM, CH, JMJ, VMKV); and Department of Veterinary Microbiology (JCDH, VM), University of Saskatchewan, Saskatoon, Saskatchewan, Canada.

Send correspondence to: Valerie M.K. Verge, PhD, Cameco MS Neuroscience Research Center/University of Saskatchewan, Saskatoon City Hospital – Rm 5800, 701 Queen St. Saskatoon, SK S7K 0M7, Canada; E-mail: valerie.verge@usask.ca

Present address: Department of Critical Care Medicine, Rady Faculty of Health Sciences, University of Manitoba, Winnipeg, Manitoba, Canada (JCDH).

Vikram Misra and Valerie M.K. Verge are co-senior authors.

This work was supported by Canadian Institutes of Health Research (CIHR) grants #74747 and #14238 to Valerie M.K. Verge and by a Natural Sciences and Science and Engineering Research Council (NSERC) of Canada grant to Vikram Misra. Jovan C.D. Hasmatali was supported by University of Saskatchewan College of Graduate and Postdoctoral Studies Scholarships

The authors have no duality or conflicts of interest to declare.

Supplementary Data can be found at academic.oup.com/jnen.

processing/activation resembles that of the UPR-associated protein, activating transcription factor 6 (ATF6) (17). Luman undergoes regulated intramembrane proteolysis releasing the basic leucine zipper domain, which translocates to the nucleus, activating target gene transcription (18–21). Luman binds cAMP response elements (16) and the UPR element in a similar capacity to the UPR protein X-box binding protein 1(XBP1) (22).

With respect to peripheral nerve injury, our labs demonstrated increased expression of ER stress markers in sensory neurons associated with each arm of the UPR. These included increases in somal and axonal CCAAT-enhancer-binding protein homologous protein (CHOP) and the ER chaperone 78-kDa glucose regulated protein (GRP78)/Binding immunoglobulin protein (BiP) levels in response to 1-day injury, with axonal UPR elements being retrogradely transported back to the cell body (7). Prior work identified Luman as a critical retrograde injury signal for axon regeneration. Luman was shown to be both synthesized and activated in the axonal ER equivalent in response to axotomy and retrogradely transported back to the cell bodies of sensory neurons in an importin-dependent manner (12). Luman was subsequently found to regulate elements of the UPR and cholesterol biosynthesis sufficient for axon growth (7). Indeed, injured neurons necessitate a coordinated UPR and increased levels of certain ER stress regulators, in particular XPB1, to improve regeneration outcomes (8).

The recent identification of genes temporally expressed in dorsal root ganglion (DRG) following sciatic nerve transection revealed that gene transcription occurs in a multiphasic pattern in response to axotomy (23). The phases coincide with initial injury and acute pre-regeneration responses to the injury, and a later chronic regeneration phase. Whether these distinct injury-associated transcriptional phases synchronize with corresponding ER stress responses is unknown. However, such knowledge may reveal opportunities of when one could intervene and bolster the neurons ability to deal with the associated ER stress. Insight into these phases may be elucidated through examination of regulators of ER stress in the injured neuron.

Because distinct transcriptional phases to the cell body response include an early stress response phase that is over by 6 hours post-injury, followed by a pre-regeneration phase that lasts until 4-day post-injury, and finally a regeneration phase that is clearly on by 7 days (23), we chose to conduct a spatiotemporal study examining whether Luman, as a regulator of adaptive ER stress, might be coordinately regulated. Furthermore, we examined how this might correlate with the intrinsic capacity of sensory neurons to grow an axon. Novel distinct phasic responses with respect to Luman expression in injured DRG neurons ipsilateral to injury were observed, with a largely parallel albeit less avid response in neurons contralateral to injury. The latter suggests that a broader systemic response to the injury also occurs. Whether these phasic alterations in Luman expression might correlate with the intrinsic ability of injury-conditioned or contralateral uninjured neurons to grow an axon in vitro was also determined. Maximal outgrowth occurred in the 2-day injury-conditioned neurons, with contralateral uninjured neurons only exhibiting increased outgrowth relative to naïve in the neurons contralateral to a 1-week injury. The findings support a role for Luman not only as a sensor of injury, but also 1 tightly linked to the distinct transcriptional phases of the cell body response associated with axon regeneration. The inferred involvement of this regulator of the UPR in the injured state highlights the significance of adaptive ER stress in this pathology and provides opportunities for enhancing the response.

MATERIALS AND METHODS

Unless otherwise stated, all reagents employed in this study were obtained from Sigma-Aldrich (Oakville, ON, Canada).

Nerve Injury Animal Model

A total of 138 male Wistar rats (Charles River Laboratories, St. Constant, PQ, Canada) weighing between 200 and 300 g, housed at room temperature on a 12-hour light-dark cycle with access to food and water, were used in this study. Animal procedures were conducted in accordance with the Canadian Council on Animal Care and approved by the University of Saskatchewan Committee on Animal Care and Supply.

Animals were given buprenorphine (Temgesic; 0.05–0.1 mg/kg) analgesic subcutaneously pre- and postoperatively. For peripheral nerve axotomy, animals were deeply anesthetized with inhalational isoflurane (Pharmaceutical Partners of Canada, Richmond, ON, Canada), 2% delivered at a rate of 2L/minute. A dorsal incision was made exposing the lumbar and sacral spinal column followed by careful dissection of surrounding bone and muscle to reveal the Lumbar segment spinal nerves. The right sciatic nerve was transected at its origins from the lumbar 4–6 (L4–L6) spinal nerves and a small 5-mm segment resected to prevent regeneration. This anatomical injury site was selected as it ensures nearly 100% injury of the L4–L6 DRG neurons. Axotomized animals were sutured closed in layers and placed in individual cages until tissue harvesting.

The injury time course was conducted by killing the animals after the predetermined post-injury timepoints of 1 hour, 1 day, 2 days, 4 days, and 1 week. Naïve control animals underwent anesthetic procedures but had no surgical intervention. Sham animals were surgically exposed and tissues were dissected out at the same postsurgical timepoints as with the nerve injured rats, with the exception that no spinal nerve was handled or injured.

For tissue analysis, a total of 4 injury time courses (naïve, 1 hour, 1 day, 2 days, 4 days, and 1 week; n = 3 rats/experimental timepoint/time course; 72 rats total) and 1 sham surgery time course (n = 3 rats/experimental timepoint/time course; 18 rats total) where the nerve was exposed but not injured were generated. Three of these injury time courses and the sham injury time course were processed for quantitative immunofluorescence data, while the remaining injury time course was processed for in situ hybridization.

Four additional time courses, naïve, 2 days, 4 days, and 1 week (n = 3 rats/experimental timepoint/time course; 48 rats total) were generated, 3 for the 24-hour intrinsic axon

growth capacity assay and 1 for quantitative real-time polymerase chain reaction (qRT-PCR).

Sample Preparation

Prior to tissue harvesting, animals were anesthetized with a Euthanyl Forte overdose (Bimeda-MTC, Cambridge, ON, Canada). The rats were perfused via the left ventricle with 100 mL of 0.1 M warm phosphate buffered saline (PBS) only for in situ hybridization studies and with PBS followed by 500 mL of ice cold 4% paraformaldehyde with 0.2% picric acid (Sigma-Aldrich) for immunofluorescence. The L4–L6 ipsilateral and contralateral DRGs were dissected promptly, postfixed (1–1.5 hours) and cryoprotected in 20% sucrose. Control and experimental tissues were embedded in the same cryomolds to ensure processing under identical conditions, covered in optimal cutting temperature compound (Sakura Finetek USA, Torrance, CA) and frozen in cooled isopentane (Sigma-Aldrich) prior to storing at −80°C until processing.

Immunofluorescence Histochemistry

The DRG tissues were sectioned serially at 6 μm on a cryostat and thaw mounted onto cooled ProbeOn Plus slides (Fisher Scientific, Ottawa, ON, Canada). Immunohistochemistry slides were air-dried, washed in PBS (3 × 10 minutes) and blocked with 10% donkey serum in 0.25% Triton-X in PBS for 1 hour at room temperature. Tissues were incubated with primary antibody, either rabbit anti-Luman (Misra Laboratory, University of Saskatchewan, Saskatoon, SK, Canada) diluted 1:400 in 2% donkey serum + 0.25% Triton X-100) (7, 12, 16), or rabbit anti-ATF-3 (1:2000, Santa Cruz Biotech, Dallas, TX) overnight in humidified containers at 4°C. All slides were also co-incubated with goat anti-LaminB (1:50, Santa Cruz Biotech), a protein localized to the nuclear envelope to allow accurate identification of the nuclear compartment, mouse anti-glial fibrillary acidic protein ([GFAP]; 1:100, Cell Signaling Technology [New England Biolabs], Whitby, ON, Canada) or mouse anti-calcitonin gene-related peptide ([CGRP]; 1:100 Abcam, Cambridge, MA). The following day, slides were washed in 0.1 M PBS (3 × 10 minutes) and incubated with Jackson ImmunoResearch (West Grove, PA) secondary antibodies, donkey anti-rabbit Cy3 (1:600), donkey anti-goat Dylight 488 (1:2000), or Alexa Fluor 488-conjugated donkey anti-mouse IgG (1:1000) for 1 hour in the dark at room temperature. Slides were washed in 0.1 M PBS (3 × 10 minutes) and coverslipped with Prolong Gold with 4', 6-diamidino-2-phenylindole (DAPI) (Life Technologies) as an additional means to LaminB to accurately identify the nuclear region. Additional slides were incubated with the omission of primary antibody and processed as above as immunofluorescence controls. Specificity of the Luman antibody was assessed via immunofluorescence or Western blot analysis with antibody aliquots pre-absorbed with cell protein isolates from Vero cells transfected with either Luman or Zhangfei, the latter a potent and efficient inhibitor of Luman activity (16, 19) that should not disrupt Luman/anti-Luman interactions (Fig. 1).

Immunofluorescence Quantification and Analysis

To ensure accurate quantification of the Luman immunofluorescence signal over cytoplasmic and nuclear regions and allow comparison between groups, the following precautions were taken: (i) each cryomold contained individual L5 DRG ipsilateral and contralateral to lesion for all injury timepoints examined, as well as naïve control ganglia. Mounting all groups on the same slide ensured processing under identical conditions and negates the impact of any slide to slide variance between groups; (ii) digital images were taken under identical exposure conditions using Northern Eclipse v7.0 software (Empix Imaging, Mississauga, ON, Canada) for all experimental groups on the same slide. Photomicrographs of immunofluorescence were taken using Zeiss Axio Imager M.1 fluorescence microscope; (iii) the injury state of all DRG used in the time course was confirmed by the presence of nuclear activating transcription factor-3 (ATF-3) (Fig. 1D); (iv) only neurons with a clearly defined LaminB-positive ring were included in the analysis, as this ensures that the neuron was sectioned through its center, allowing for accurate assessment of cell size and nucleus-associated immunofluorescence. The corresponding image of the LaminB immunofluorescence for the neurons being analyzed was opened on the same screen as the Luman immunofluorescence to allow for this assessment; and (v) great care was taken when tracing the neuron so as not to include any immunofluorescence associated with the Luman-positive perineuronal region, which in naïve neurons is associated with GFAP-positive satellite glial cells (Fig. 2B).

The intensity of the immunofluorescence signal for cytoplasmic and nuclear regions (average gray/micron^2) for each neuron and neuronal diameter were measured using Northern Eclipse v7.0 software (Empix Imaging) by an evaluator blinded to the experimental condition. Scatterplots and line graphs were constructed in GraphPad Prism v5.0 (GraphPad Software, La Jolla, CA) and statistical significance between timepoints and conditions were assessed using the Kruskal-Wallis 1-way ANOVA with Dunn's post-test analysis or the Mann-Whitney t-test, with statistical significance at p values <0.05.

To assess the incidence of CGRP expression in the subpopulation of sensory neurons displaying moderate to high levels of Luman immunofluorescence, L5 DRG sections from 4 naïve rats were processed for dual Luman/CGRP immunofluorescence. Those neurons with moderate to high levels of Luman immunofluorescence were then identified in the sections followed by assessment of whether there was detectable CGRP immunofluorescence in the same neurons. The incidence of co-expression was then calculated as a percentage ± SEM along with the incidence of those neurons that are CGRP-expressing without moderate to high levels of Luman immunofluorescence and those with moderate to heavy Luman immunofluorescence and no detectable CGRP.

Western Blot

Proteins were extracted from tissue and cell culture samples with ice cold radioimmunoprecipitation assay buffer containing protease inhibitor cocktail (Sigma-Aldrich). These

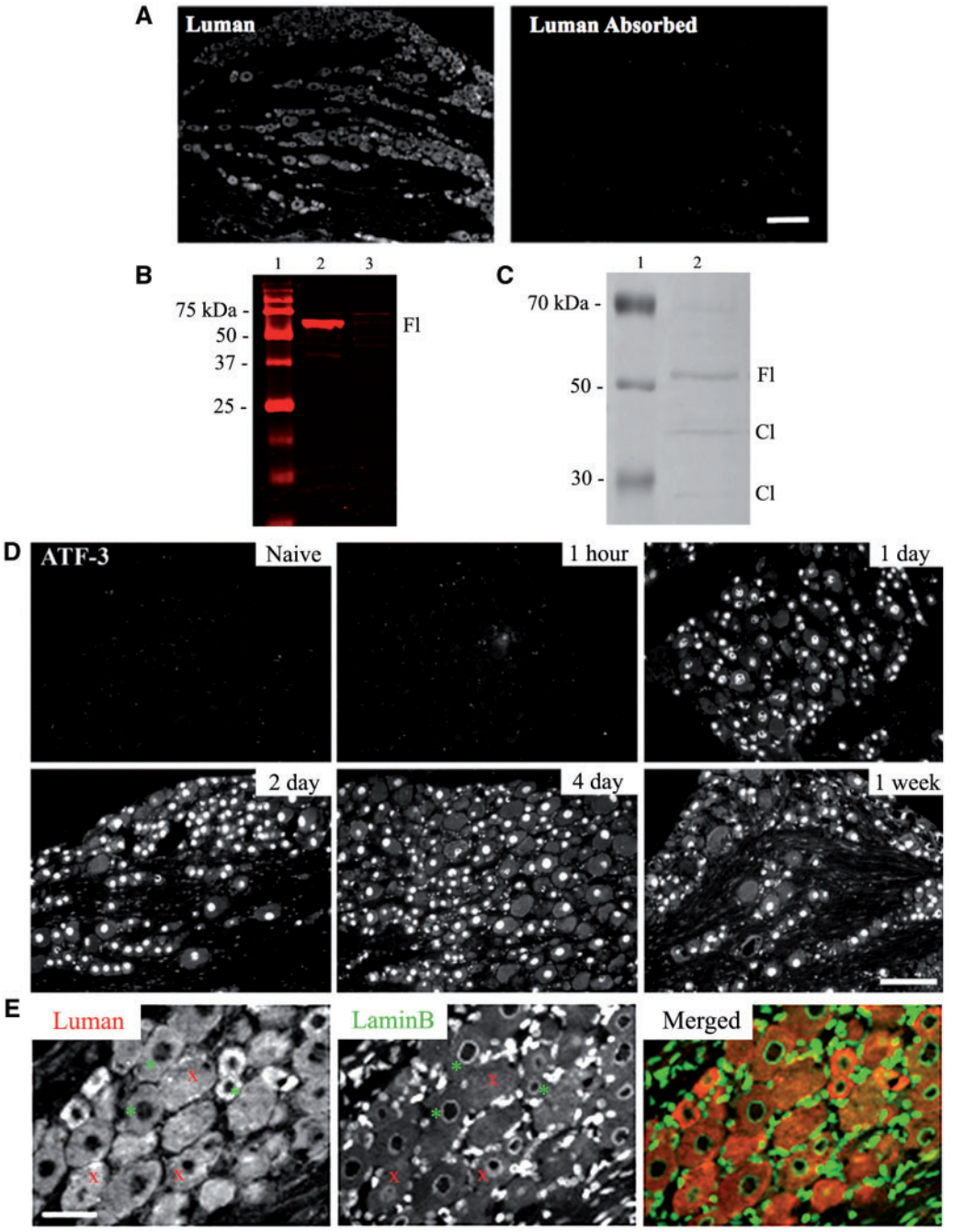

FIGURE 1. Luman antibody and injury specificity controls. **(A)** Photomicrographs of L5 dorsal root ganglion (DRG) (6-μm sections) processed for immunofluorescence detect Luman protein with anti-Luman rabbit serum (left) and anti-Luman absorbed with cell protein isolates from Luman-transfected Vero cells. Scale bar = 160 μm. Note: Absorption of anti-Luman abolishes immunofluorescence staining. **(B)** Western blot analysis of anti-Luman rabbit serum-treated membrane of electrophoresed protein extracts from Vero cells transfected with Luman (lane 2) or Zhangfei (lane 3). Molecular weight marker (lane 1). Note: In the Luman-transfected cell extract, anti-Luman recognizes a single band of approximately 60 kDa, the suspected molecular weight of unprocessed Luman, while unable to detect any identifiable antigen in the Zhangfei-transfected cell extract at its expected molecular weight of approximately 30 kDa. **(C)** Western blot analysis of protein extracts from naïve L4 and L5 DRG (lane 2). Molecular weight marker (lane 1) Note: Anti-Luman recognizes unprocessed full-length Luman (Fl) at approximately 60 kDa and 2 additional faint bands of approximately 40 and 15 kDa, the predicted molecular weights of Luman protein cleavage products (Cl). **(D)** L5 DRG sections (6 μm) processed to detect injury-associated ATF-3 protein in DRG sections ipsilateral to 1-hour, 1-day, 2-day, 4-day, and 1-week L4–L6 spinal nerve transection or naïve controls. Scale bar = 150 μm. Injury state is confirmed by presence of nuclear ATF-3 immunofluorescence, detectable by 1-day post-injury. **(E)** To accurately delineate cytoplasmic and nuclear compartments, all tissue was dually processed for Luman (red) and LaminB (green)

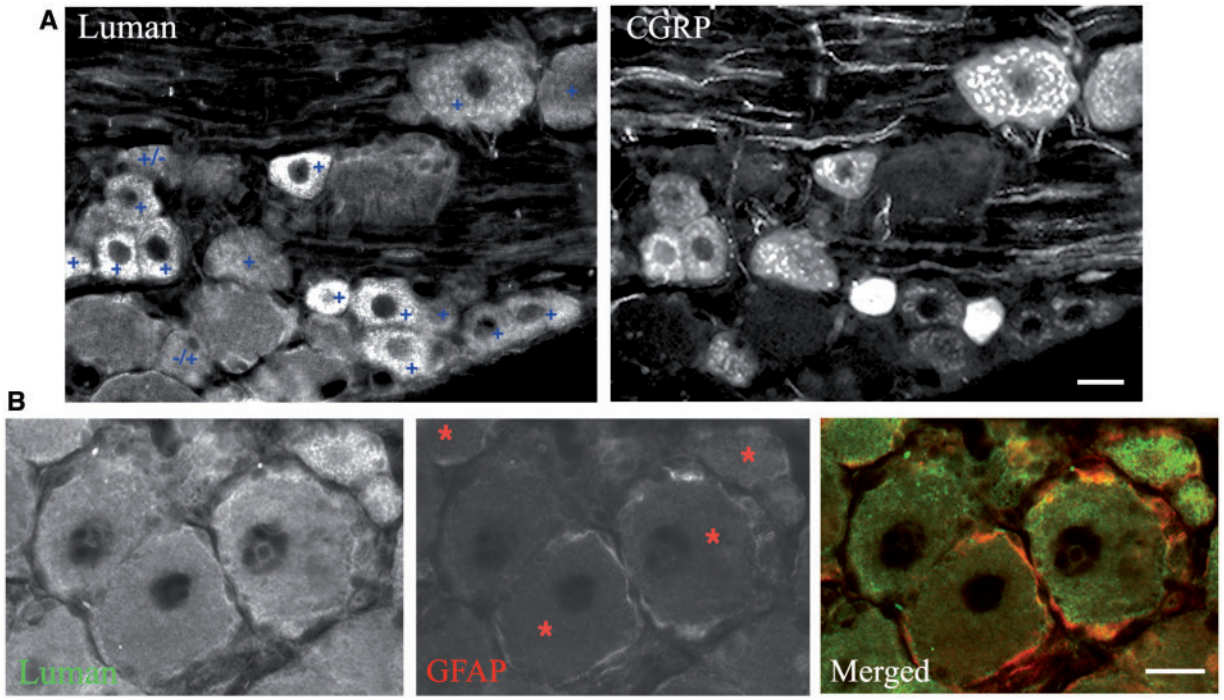

FIGURE 2. Characterization of Luman immunofluorescence in dorsal root ganglion (DRG). **(A)** Representative image of a L5 DRG section from a naïve rat processed for dual immunofluorescence to examine incidence of moderate to high Luman immunofluorescence signal (+) in calcitonin gene-related peptide (CGRP)-positive neurons. Note that the majority of neurons with moderate to heavy Luman immunofluorescence (+) have detectable levels of CGRP, with only the rare Luman neuron not expressing detectable CGRP (+/−) or the rare CGRP-positive neuron not expressing moderate to high levels of Luman immunofluorescence (−/+). Scale bar = 25 μm. **(B)** Representative image of a L5 DRG section from a naïve rat processed for dual immunofluorescence to examine Luman expression in glial fibrillary acidic protein (GFAP)-positive perineuronal satellite glial cells. Note the colocalization of these 2 markers in the perineuronal cells of neurons identified with red asterisk. Scale bar = 25 μm.

samples included L4–L6 DRG from naïve animals and Vero cells grown in culture. For Luman antibody specificity controls, Vero cells were maintained in Dulbecco's modified Eagle's medium (Invitrogen, Carlsbad, CA), with 10% newborn calf serum, 100 unit/mL penicillin, and 100 mg/mL streptomycin at 37°C in a humidified incubator with 5% CO_2. The day prior to transfection, Vero cells were seeded into 6-well plates at a density of 5×10^5cells/collagen-coated well. Cells were transfected with 1 μg of pcDNA3.1, pcLuman or pcZhangfei, using Lipofectamine (Fisher Scientific) in 6-well plates as per the manufacturer's instructions.

Twenty micrograms of DRG or Vero cell extracts were electrophoresed on a 10% or 12% SDS polyacrylamide gels, respectively, along with a protein molecular size marker (LI-COR Biosciences, Lincoln, NE) and then transferred onto a polyvinylidene fluoride membrane (Bio-Rad Laboratories, Ltd, Mississauga, ON, Canada) by semidry electroblotting for 15 minutes in cold transfer buffer (25 mM Tris, 192 mM Glycine, 20% methanol) at 15 V using a Bio-Rad Trans-Blot apparatus. Membranes were blocked with blocking buffer (LI-COR Biosciences) at room temperature for 1 hour. Membranes were then incubated with primary antibodies (Luman 1:4000) in LI-COR Odyssey blocking buffer with 0.1% Tween 20 overnight at 4°C, followed by incubation with Goat anti-Rabbit LI-COR IRDye 680 (1:10 000, LI-COR Biosciences) secondary antibodies for 1 hour at room temperature. Proteins were visualized by the Odyssey Infrared Imaging System (LI-COR Biosciences). Mouse anti-GAPDH (1:10 000) was used to detect GAPDH loading control. Membranes were then rinsed in distilled water and scanned on the Li-Cor Odyssey 9120 infrared scanning system (LI-COR Biosciences).

FIGURE 1. Continued
immunofluorescence, the latter recognizing the nuclear envelope. Only neurons with a clearly defined LaminB ring were analyzed (examples-*), as they identify cells sectioned through their center with clear cytoplasmic and nuclear compartments; those without defined rings were not (examples-**x**). Scale bar = 75 μm.

In Situ Hybridization

Oligodeoxyribonucleotide (OligoDNA) 48 mer probes were synthesized complementary to and selective for Luman mRNA (5′-TATCTCAATCACCATGGCTTGA AGCTTCCT CAGTTGATCTAGAAGGGA-3′) (University of Calgary DNA Services, Calgary, AB, Canada). All cDNA regions used were checked against the GenBank database (NIH, at the Internet site: www.ncbi.nlm. nih.gov); no greater than 60% homology was found to sequences other than the selected transcript. Labeling of probe with ^{35}S-dATP (Perkin Elmer, Waltham, MA) and terminal transferase enzyme (Amersham, Canada) was performed in a terminal transferase buffer, containing sodium cacodylate 500 mM, CoCl2 (pH 7.2) 10 mM, mercaptoethanol 1 mM, for 1.5–2 hours at 37°C. The reaction was halted with 500 μL, 0.1 M Tris HCl (pH 8.0), after which the probe was purified through a NENSORB-20 column (New England Nuclear, Boston, MA), and dithiothreitol added to a final concentration of 10 mM. The radioactivity was measured and the labeled probe was stored at 4°C.

All steps were performed under RNase free conditions. The slides were air-dried and postfixed in 4% PF (20 minutes), washed in PBS (3 × 5 minutes), treated with proteinase K at 37°C (20 μg/mL; 7–8 minutes), rinsed in PBS (5 minutes), fixed in 4% PF (5 minutes), rinsed in PBS (2 × 5 minutes), rinsed in diethyl pyrocarbonate (0.1%) –H_2O (5 minutes), and dehydrated in increasing ethanol concentrations (70%, 90%, 100%; approximately 1 minute in each). Sections were hybridized with radiolabeled probe at a concentration of 10^7 cpm/mL in a hybridization solution consisting of 50% formamide, 4× saline sodium citrate ([SSC]; 1 × SSC = 0.15 M NaCl, 0.015 M sodium citrate), 1 × Denhardt's solution (0.02% bovine serum albumin [BSA], 0.02% Ficoll and 0.02% polyvinylpyrrolidone), 10% dextran sulfate, 0.5 mg/mL salmon sperm DNA, 1% sarcosyl and 0.2 M dithiothreitol. Hybridization with approximately 100 μL hybridization solution/slide was conducted overnight at 43°C in air-sealed, humidified chambers to prevent evaporation. Following hybridization, the slides were washed in 1 × SSC (4 × 15 minutes, 55°C, and an additional 30 minutes, room temperature), dipped twice in distilled water, dehydrated in ascending ethanols, and air-dried. Slides were dipped in Kodak NTB2 photo emulsion (diluted 1:1 in distilled water, Kodak Canada, Toronto, ON, Canada) to generate autoradiograms. After 4–8 weeks exposure, the slides were developed in Kodak D19 (3–5 minutes), rinsed in water, fixed in Kodak rapid fix (5 minutes), and rinsed in water (20 minutes). For darkfield viewing and photography, the slides were left unstained, whereas slides for brightfield examination were counterstained with 0.5% toluidine blue (in an acetate buffer; pH 4–4.5), and mounted with Permount (Fisher Scientific) and a coverslip. The specificity of hybridization signal for the individual probes was determined by hybridization of adjacent 6-μm sections with labeled probe with the addition of either 1000-fold excess corresponding unlabeled probe, which abolished the signal, or 1000-fold excess of a dissimilar unlabeled probe of the same length and similar GC content, which left the signal unchanged from that observed with labeled probe alone. Luman oligonucleotide probe specificity controls were previously published (24).

Quantitative Real-Time Polymerase Chain Reaction

L4 DRG ipsilateral and contralateral to injury and naïve control L4 DRG were collected in RNAlater (Sigma-Aldrich) (1 DRG per tube containing 500 μL) and stored at −80°C. RNA was extracted from each DRG (n = 3 rats/condition/timepoint) using the Qiagen RNeasy Mini Plus kit (Qiagen, Mississauga, ON, Canada) as per manufacturer's instructions; RNA concentration was determined using Life Technologies Qubit RNA HS Assay Kit and Qubit 3.0 Fluorometer as per manufacturer's instructions. Isolated RNA was then reverse-transcribed to cDNA using Qiagen QuantiTect Reverse Transcription Kit (Qiagen). Luman qPCR was performed using Agilent Stratagene MX3005P and Qiagen QuantiFast SYBR Green PCR Kit. Luman qPCR primers were as follows: 5′-TGTGCCCGCTGAGTATGTTG-3′ and 5′-AGAAGGTCG-GAGCCTGAGAA-3′ (24). Data were analyzed using the ΔΔCt method in Microsoft Excel and 2-tailed p values were calculated using the unpaired t-test; p value less than 0.05 was considered significant. All qRT-PCRs satisfied MIQE guidelines. Rictor and ANKRD27 served as normalizers as per Gambarotta et al (25).

Adult DRG Culture and Axon Outgrowth Assay Quantification

Naïve, 2-day, 4-day, or 1-week L4–L6 spinal nerve injured rats were deeply anesthetized and killed, followed by removal of L4–L6 DRGs. DRG trimmed of their rootlets were treated with 0.25% collagenase for 1 hour (37°C), dissociated with 2.5% trypsin for 30 minutes (37°C). Neurons were further purified by placing on the top of a 3-mL 15% BSA solution and then spun at 850 rpm for 20 minutes at 4°C before counting and plating dissociated neurons on laminin- (1 μg/mL) and poly-D-lysine-coated (25 μg/mL) coverslips at 5000 cells/coverslip/well in 6-well plates (BD Biosciences, San Jose, CA) in Dulbecco's Modified Eagle Medium (Sigma-Aldrich). Cytosine β-D-arabinofuranoside (10 μM, Sigma-Aldrich) was added to inhibit nonneuronal cell proliferation.

After 24 hours, the cultures were immunostained with anti-βIII-tubulin to assess total axon/neurite length/neuron. Briefly, the culture coverslips were washed with PBS, fixed for 30 minutes in 2% paraformaldehyde, blocked for 1 hour at room temperature with Sea Block (ThermoFisher Scientific), then incubated in primary antibody mouse anti-βIII-tubulin (1:800, Millipore, Temecula, CA) in 10% Sea Block, 0.1% triton in 0.01 PBS overnight at 4°C. The next day, the coverslips were washed and incubated in Donkey anti-mouse AlexaFluor 594 (1:1000; Abcam, Cambridge, MA) to visualize βIII-tubulin immunopositive neurons and their neurite outgrowth.

Total axon/neurite length/neuron (identified by βIII immunofluorescence) was calculated for all neurons in each of approximately 70–80 random fields per experimental timepoint for each of the 3 experimental time courses/replicates, resulting in 200–250 neurons being analyzed per experimental timepoint. For quantitative analysis of axon outgrowth in each experimental group, random fields were digitally photographed using a Zeiss Axioskop microscope using the 20× objective. Axon outgrowth analysis was carried out using

Neurobin (Northern Eclipse, Empix Imaging). The Kruskal-Wallis nonparametric ANOVA test (Prism, GraphPad Software, La Jolla, CA) was used to compare the mean axon length for each treatment group with Dunn's post-test analysis. Statistical significance was accepted at $p < 0.05$ level.

RESULTS

The specificity of the anti-Luman antibody was assessed immunohistochemically on DRG tissue sections incubated with anti-Luman or anti-Luman serum absorbed with cell protein isolates from Luman-transfected Vero cells (Fig. 1A). Absorption of the antibody resulted in near elimination of immunofluorescence staining as compared to tissue samples processed with anti-Luman alone. Western blot analysis further characterized the anti-serum specificity. Membranes of electrophoresed lysates of cells transfected with Luman (Fig. 1B, lane 2) or Zhangfei (Fig. 1B, lane 3) were incubated with anti-Luman serum. In the Luman-transfected Vero cell extract, anti-Luman recognized a single band of approximately 60 kDa, the predicted molecular weight of unprocessed Luman, while unable to detect any identifiable antigen in the Zhangfei-transfected cell extract at the expected MW of approximately 30 kDa. In protein extract from naïve DRG, Luman anti-serum also recognized the unprocessed/full-length form of Luman and low levels of 2 additional bands in rat DRG extract of approximately 40 and 15 kDa, the predicted molecular weights of Luman protein cleavage products (Fig. 1C).

Prior to conducting the Luman spatio-temporal analysis, the injury state of the DRG tissue was confirmed in 2 ways: visually at the time of dissection, and by the upregulation and nuclear localization of ATF-3, detectable in the nuclei of DRG neurons injured for 1 day or longer (26, 27). All injured DRG met these criteria and thus could be included in the analysis (Fig. 1D). Furthermore, as the unstable catalytic domain of Luman is cleaved and translocates to the nucleus in response to stress events, the nuclear envelope protein LaminB was used to delineate the nuclear region to allow for quantification of alterations in Luman localization to this cellular compartment. Only neurons with complete and distinct rings of LaminB staining around the nucleus were analyzed. This assures that the neuron was sectioned through its center and allows for both accurate determination of neuron size and maximal visualization of the nucleoplasm (Fig. 1E). Nuclear DAPI staining was also used to confirm presence of nucleoplasm. Finally, to ensure accurate and reliable assessment of relative changes in Luman immunofluorescence signal from 1 experimental condition to the next, the cryomolds to be sectioned contained 1 DRG from each experimental group analyzed. This allows for all experimental conditions to be represented on the same slide and processed for immunofluorescence in an identical manner, negating any potential slide to slide variance in immunofluorescence levels.

Characterization of Luman Expression in Naïve DRG

While some level of Luman immunofluorescence/expression is detectable in all sensory neurons, the population of naïve sensory neurons with moderate to high levels is primarily small to medium in size, with the occasional large-size neuron (Figs. 1 and 2). This is the size distribution for nociceptive neurons and is most consistent with the nerve growth factor (NGF)-responsive subpopulation of nociceptors, which is best characterized by its expression of the nociceptor-associated neuropeptide CGRP (28, 29). Thus, the incidence of CGRP co-expression was examined in the subpopulation of naïve sensory neurons displaying moderate to high Luman immunofluorescence. Neurons displaying moderate to high levels of Luman immunofluorescence were first identified in sections of L5 DRG from 4 naïve animals that had been processed for dual Luman/CGRP immunofluorescence (Fig. 2A). The incidence of Luman/CGRP co-expression was determined, followed by assessment of how many neurons with detectable CGRP did not express moderate to high levels of Luman immunofluorescence. A high incidence of CGRP co-expression was found in neurons with moderate to high Luman immunofluorescence (90.71% ± 2.54% [SEM] of sensory neurons). This population represents 95.76% ± 2.76% (SEM) of CGRP-positive neurons detected. Thus, the NGF-responsive, CGRP-expressing subpopulation of primary sensory neurons displayed moderate to high levels of Luman immunofluorescence, suggesting a potential role for Luman in nociception.

To determine whether the rings of bright Luman immunofluorescence observed in the perineuronal region localized to satellite glial cells, additional sections of naïve tissue were dually processed for Luman and GFAP, a phenotypic marker of this cell population. Qualitative examination of the resulting co-expression revealed that the bright rings of perineuronal Luman immunofluorescence colocalized with GFAP (Fig. 2B) in the 4 animals examined, supporting that this subpopulation of satellite glial cell does indeed express Luman. It also highlights the importance of not including this region when determining the level of neuronal Luman immunofluorescence signal.

Axotomy Induces Biphasic Changes in Luman Expression and Nuclear Localization in Injured Sensory Neurons

Distinct transcriptional phases in the response of sensory neurons to nerve injury have recently been described in (23). This made us posit that Luman, in its role in sensing perturbations in the homeostatic state of sensory neurons, might be regulated in a manner that reflects these nerve injury-associated phasic transitions. The effect of nerve transection on Luman expression in sensory neuron was investigated by axotomizing the sciatic nerve of male Wistar rats at the level of the L4–L6 spinal nerves to assure complete transection of virtually all axons within the ganglion. In situ hybridization, RT-qPCR and immunofluorescence were used to assess alterations at the transcript and protein levels. Luman immunofluorescence levels in naïve ganglia were higher in small-medium diameter neurons and the occasional large-size neuron with low-moderate nuclear staining in a small fraction of these cells (Fig. 2A).

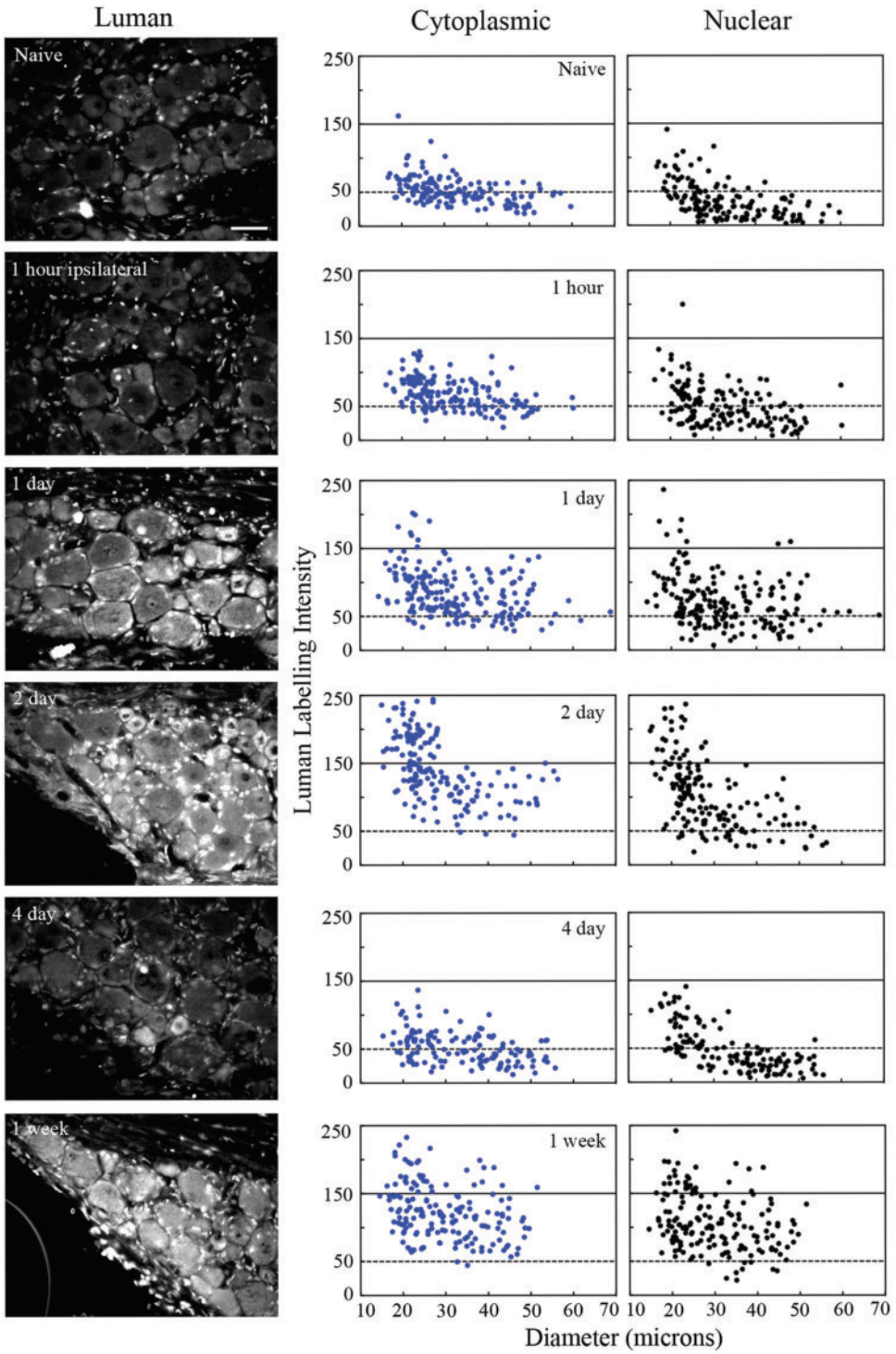

FIGURE 3. Unilateral peripheral nerve injury alters Luman levels detected in axotomized ipsilateral dorsal root ganglion (DRG) neurons. Left Column: Representative immunofluorescence photomicrographs of L5 DRG sections (6 μm) detecting Luman protein in DRG ipsilateral to L4-L6 spinal nerve transection rats were at 1-hour, 1-day, 2-day, 4-day and 1-week post-injury. Scale bar = 50 μm. Naïve animals served as controls. Sections shown were all mounted on the same slide to ensure processing under identical conditions and are those for which the quantification is shown Right column: Representative scatterplots depicting relative changes in Luman immunofluorescence signal over individual neuronal cytoplasmic and nuclear regions as related to neuron size. Experimental states as indicated. Dashed lines divide the plots into low versus moderate to heavily labeled populations (n = 181–206 neurons analyzed per condition/animal). A total of 3 separate animals were analyzed in this manner per condition.

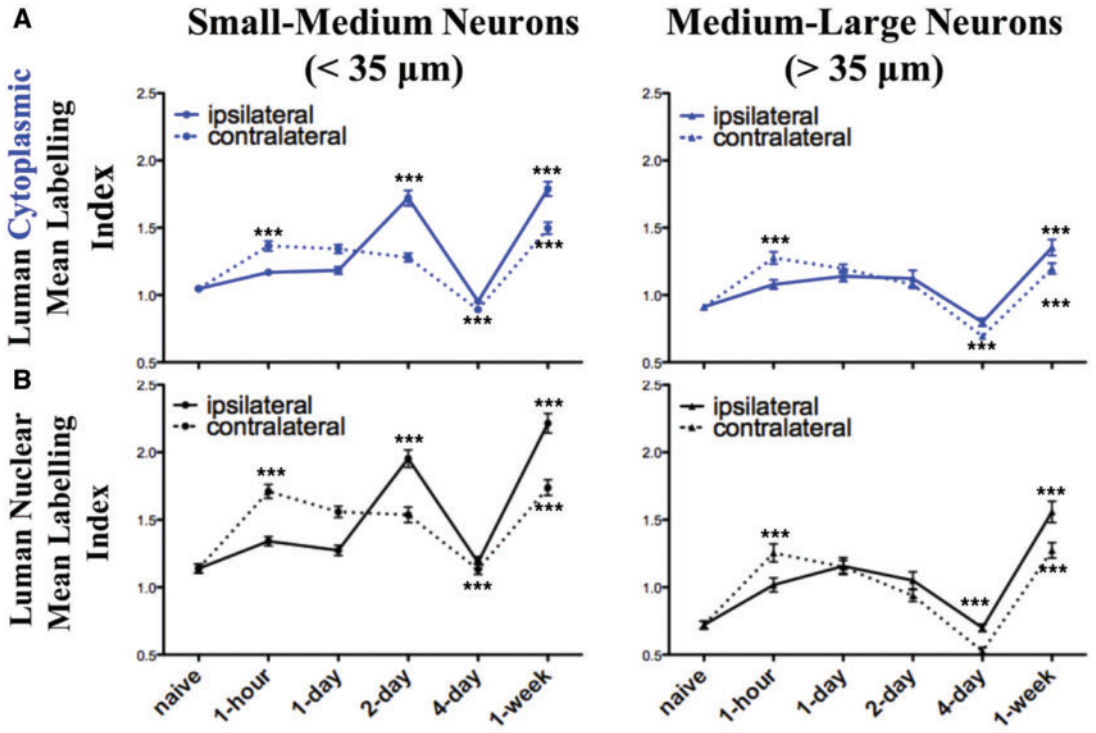

FIGURE 4. Peripheral unilateral axotomy results in bilateral biphasic alterations in Luman protein immunoreactivity in both injured and contralateral uninjured dorsal root ganglion (DRG) neurons. Summary line graphs of alterations in the mean + SEM. cytoplasmic (**A**, blue) and nuclear (**B**, black) Luman immunofluorescence intensity levels as normalized to the mean naïve control value on the same slide. Data were subdivided into that observed in small- and medium-sized (<35 µm, column 1) and medium- and large-sized (>35 µm, column 2) DRG neurons ipsilateral (injured—solid line) and contralateral (uninjured—dashed line) to injury at timepoints as indicated (n = 181–206 neurons analyzed per timepoint per animal analyzed), with 3 rats/experimental condition assessed for each data point. ***$p < 0.001$ ANOVA with Dunn's post-test analysis for change relative to previous timepoint. Note: relative changes in nuclear localization parallel those observed for the cytoplasmic staining.

At 1-day post-axotomy, neurons ipsilateral to lesion had higher levels of Luman immunofluorescence (Figs. 3 and 4) and mRNA (Fig. 6) compared to naïve controls with visible translocation of Luman immunofluorescence to the nuclei of small neurons. The first peak in Luman immunofluorescence signal was observed at 2-day post-injury, when high cytoplasmic and nuclear immunoreactivity was clearly evident in the subset of small- and medium-sized neurons, with larger neurons demonstrating only slightly increased levels over naïve controls (Figs. 3 and 4); increases in transcript levels were also found to be significantly different from naïve at this timepoint (Fig. 6). Qualitatively, parallel changes in nuclear Luman immunofluorescence levels (confirmed by DAPI and LaminB staining) in the perineuronal regions were also observed.

By 4-day post-injury, dramatically decreased Luman immunofluorescence signal was observed across all size ranges of neurons with only a few neurons appearing to be moderately labeled. The decreased levels at this timepoint were similar to those obtained in the naïve state for both cytoplasmic and nuclear compartments (Figs. 3 and 4). In contrast, Luman mRNA remained higher than naïve controls in DRG ipsilateral to 4-day spinal nerve lesion (Fig. 6). Thus, the decrease in immunofluorescence observed at 4 days is likely attributable to regulation at the post-transcriptional level. In contrast, by 1-week post-injury, a second peak in Luman immunofluorescence was observed. This time, however, the elevated expression was not restricted to the small- to medium-size neurons. Instead, the elevated immunofluorescence signal was evident in neurons across all size ranges of neurons (Figs. 3 and 4). These observations suggest that as result of injury, ER stress may be initially higher in small to medium size, presumably nociceptive neurons, then decrease and rise for a second time after 4-day injury to higher levels in all size ranges of neurons, including the larger-sized neurons with presumed proprioceptive and/or mechanoreceptive functions.

Unilateral Axotomy Affects Contralateral Luman Expression and Localization

How broadly the injury response is communicated is still a subject of debate. Unilateral axotomy has been documented to result in altered protein expression on the uninjured/contralateral side (30–32). But whether the stress of injury is reflected in altered Luman expression in uninjured contralateral neurons has yet to be investigated. We found that unilateral sciatic L4–L6 spinal nerve injury resulted in changes in Luman immunofluorescence signal and nuclear localization in DRG contralateral to injury that were rapid, biphasic, and largely paralleled that which was observed in the DRG ipsilateral to injury, albeit at lower levels (Figs. 3–

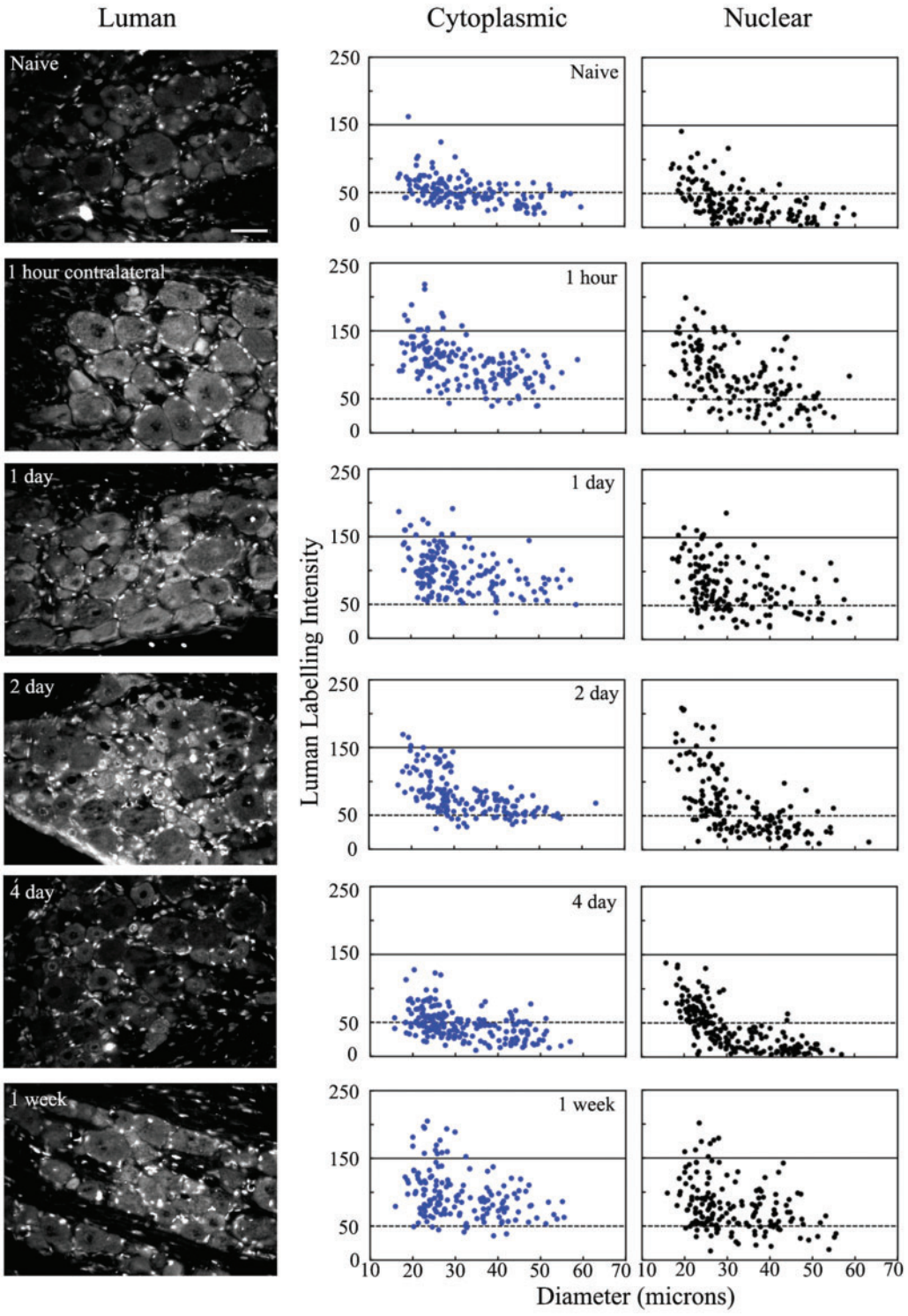

FIGURE 5. Unilateral peripheral nerve injury alters Luman protein levels in uninjured dorsal root ganglion (DRG) neurons contralateral to injury. Left Column: Representative photomicrographs of L5 DRG sections (6 μm) processed for immunofluorescence to detect Luman protein in DRG contralateral to 1-hour, 1-day, 2-day, 4-day and 1-week injury. Sections shown were all mounted on the same slide to ensure processing under identical conditions and are those for which the quantification is shown. Scale bar = 50 μm. Naïve animals served as controls. Right Column: Representative scatterplots depicting relative changes in Luman immunofluorescence signal over neuronal cytoplasmic and nuclear regions as related to neuron size. Experimental states as indicated. Dashed lines divide the plots into low versus moderate to heavily labeled populations (n = 181–204 neurons analyzed per animal per condition). A total of 3 separate animals were analyzed in this manner per condition.

5). While the first peak in Luman immunofluorescence in DRG neurons ipsilateral to lesion occurred at 2-day post-lesion, the first peak in Luman expression was evident at the 1-hour timepoint in DRG neurons contralateral to injury, with elevated neuronal cytoplasmic and nuclear levels detected. In addition, there appeared to be elevated Luman immunofluorescence in the nuclei of perineuronal cells at this early timepoint. This heightened expression pattern was still evident at 1 day (Figs. 4 and 5). By 2 days, a slight decline in Luman levels was discernible. Once again, significantly lower levels found in the 4-day-injured DRGs, with levels reduced to those observed in naïve neurons (Figs. 4 and 5). However, unlike the ganglia ipsilateral to lesion, the Luman detected in the perineuronal cell (presumably satellite glial cell) nuclei at 4-day post-injury were still quite elevated, albeit lower than at the first peak 1-hour post-injury (Fig. 5). These changes in immunofluorescence were not mirrored by similar changes in mRNA expression, as only small insignificant variances in expression were detected using both in situ hybridization and RT-qPCR approaches. While this suggests that the contralateral increases or reductions in expression post-injury might be through protein stability or increased or decreased translation, 1 cannot rule out impacts on mRNA stability or translational efficiency (Fig. 6).

Luman Levels Are Not Discernibly Altered by Sham Surgery

Because there is a robust increase in Luman detected in the nuclei and cytoplasm of neurons and perineuronal cells in contralateral ganglia across all size ranges of neurons, we had to ascertain whether the contralateral changes in expression were due to systemic stress response associated with the surgical exposure or the actual spinal nerve lesions. Thus, sham surgeries were performed and qualitatively assessed at each timepoint for alteration Luman expression and localization in L4, 5 DRG ipsilateral or contralateral to the surgical exposure site. Qualitative analysis of ipsilateral or contralateral L5 DRG sections processed for Luman immunofluorescence ($n = 3$ animals/timepoint) did not reveal any discernible changes relative to naïve controls, suggesting that the changes observed in the axotomy time course were due to the nerve injury imposed and not the surgical stress state (Supplementary Data Fig. S1).

The Intrinsic Axon Growth Capacity of Sensory Neurons Ipsilateral and Contralateral to a Conditioning Injury Is Temporally Altered

In vitro growth assays are an effective way to evaluate how in vivo experimental conditions alter the intrinsic axonal/neurite growth capacity of adult sensory neurons (12, 33, 34). If conducted acutely, the assay reflects the growth state of the neurons at the time of culturing. Smith and Skene noted that a transition occurs after 24 hours in vitro whereby dissociated naïve neurons begin to switch their form of axon growth from an arborized toward an elongating form of growth (33). For this reason, all growth assay experiments in our study were terminated at 24 hours, allowing for sufficient outgrowth from the neurons without having to factor in culturing-induced alterations in growth competence.

Quantitative and qualitative evaluation of the intrinsic growth competence of 2-day, 4-day, or 1-week injury-conditioned neurons revealed that 2-day injury-conditioned neurons exhibited the highest level of 24-hour axon/neurite outgrowth; this was significantly greater than naïve and the 2 other injury timepoints examined (Fig. 7). This peak in outgrowth corresponds with the first peak in Luman cytoplasmic and nuclear immunofluorescence observed in the injured neurons (Figs. 3 and 4). There was significantly reduced axonal outgrowth in the 4-day injury-conditioned neurons relative to the 2-day timepoint (Fig. 7) and this correlates with the dramatic decline in Luman levels observed (Figs. 3 and 4). However, this level of intrinsic outgrowth did not increase significantly beyond that of the 4-day injury in the 1-week injury-conditioned neurons, despite significantly increased Luman expression and nuclear localization equivalent to levels seen in the 2-day-injured neurons (Figs. 3 and 4).

We next examined whether the altered Luman expression and nuclear localization observed in contralateral uninjured L4–L6 DRG neurons correlated with alterations in intrinsic axon/neurite growth capacity and found that neither the 2-day nor the 4-day contralateral neurons exhibited a similar form and extent of outgrowth as that seen in naïve neurons (Fig. 7). However, 1-week-prior injury of sensory neurons resulted in significantly longer growth relative to naïve in the L4–L6 uninjured contralateral DRG neurons (Fig. 7). Qualitatively, this outgrowth was predominantly of the elongating and not the arborized form, which is notable because the predominantly elongating form of growth had only been described for the injury-conditioned neurons in the Smith and Skene study (33). In that study, the controls were always naïve neurons and not the uninjured contralateral neurons.

DISCUSSION

Our previous studies revealed that axotomy results in early increases in axonal Luman synthesis, cleavage and the retrograde transport of the activated Luman signal back to the cell body. There it serves as a critical early retrograde injury signal regulating the intrinsic ability of 1-day-injured sensory neurons to regenerate an axon through the regulation of the UPR and cholesterol biosynthesis (7, 12). Extended temporal analysis of the axotomy response in this study reveals clear biphasic changes in Luman cytoplasmic immunofluorescence and nuclear localization at the neuronal and perineuronal cell levels, both ipsilateral and contralateral to injury. This suggests that in addition to axonal ER-associated Luman "sensing" the injured state and encoding a retrograde signal, alterations in neuronal and perineuronal Luman expression likely serve as part of an adaptive response that may help mitigate regeneration-associated ER stress or UPR challenges and promote regenerative growth during the distinct regeneration phases.

A notable finding was that there is a potential role for Luman in the cell body response of DRG neurons associated with early, acute and chronic phases of axotomy. This injury response is also sensed in a largely parallel albeit lesser man-

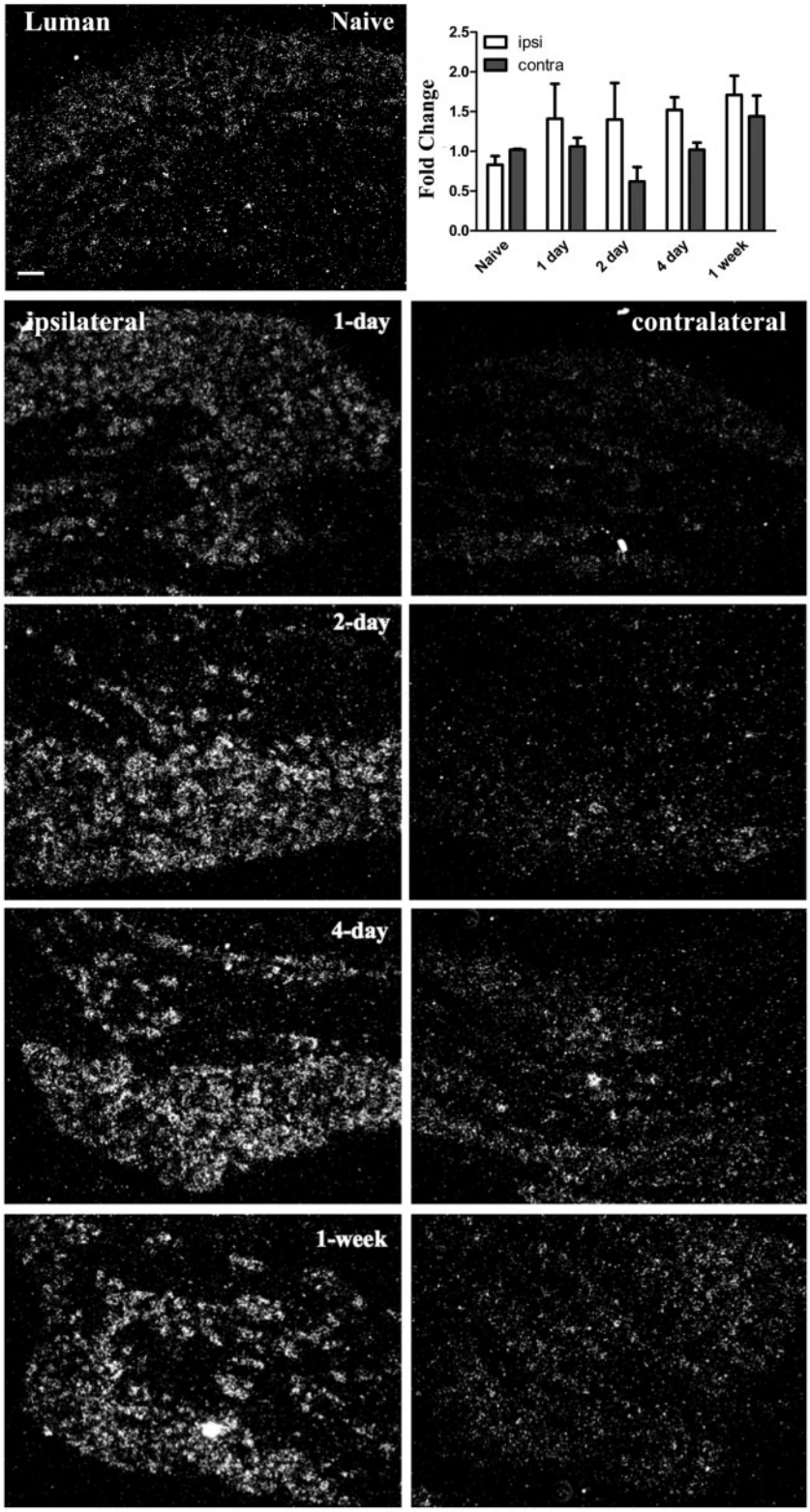

FIGURE 6. Unilateral peripheral axotomy alters Luman mRNA expression in dorsal root ganglion (DRG) neurons ipsilateral to injury. Representative darkfield photomicrographs of L5 DRG sections (6 μm) or DRG processed for radioisotopic in situ hybridization or qRT-PCR (graph insert), respectively, to visualize and quantify alterations in Luman transcript expression relative to naïve in ipsilateral-injured and contralateral-uninjured DRG. Ipsilateral (left column) and contralateral (right column) DRG sections are from DRG 1-hour, 1-day, 2-day, 4-day, and 1-week post-injury as indicated. Top left: Naïve animals served as

ner contralateral to injury, showing that the distinct transcriptional phases observed in the injured neurons must have also parallel systemic influences. Because the impact of injury on Luman levels in neurons contralateral to injury was not observed in sham animals, this supports that surgical stress unlikely contributed to the altered contralateral expression; rather, it is a response to the injury. Beyond the phasic alterations in Luman expression, we also discovered that the intrinsic capacity for sensory neurons to grow an axon/neurite changes temporally after injury. Because this intrinsic plasticity is maximal for the 2-day injury-conditioned neurons, this may be an optimal time for surgical repair however this remains to be determined. Surprisingly, we also found a significantly increased capacity for axonal/neurite growth in uninjured neurons contralateral to 1-week injury to grow, with qualitative assessment of this mode of growth being more consistent with that normally observed in injured neurons. These are significant findings, as they reveal that axotomy has systemic impacts that are phase-specific and extend beyond the affected injured neuron.

Luman Expression in Sensory Neurons and Its Role in the Nerve Injury Response

Luman is a known regulator of the UPR (20, 35), a role recently extended to injured sensory neurons and 1 that has been linked to the intrinsic ability of an injured axon to regrow (7). Furthermore, this association with ER stress is the likely explanation for the robust changes in expression observed in injured neurons. Peripheral nerve damage causes a phenotypic shift in sensory neurons from a "transmitting" cell to one of "regeneration" with a goal of producing new fibers and growth back to previously innervated areas (36). Sensory neurons upregulate a myriad of regeneration-associated genes critical to axon growth, including other transcription factors such as ATF-3 (26, 27) or c-Jun (37), as well as growth-associated proteins (34, 38). This cell body response causes a significant protein burden to the cell and evidence suggests that proper protein processing, ER stress, and the UPR are critical especially during regenerative growth. Studies show a correlation between PNS disease states and elevated levels of ER stress markers. For example, damage to sciatic nerves increased expression of the chaperone protein GRP78/BiP in the soma of non-degenerating neurons and the transcription factors XBP1s and ATF4 in degenerating motoneurons (5, 39). There are also reports of peripheral nerve damage upregulating other chaperone proteins and ER foldases, types of chaperones that assist in protein folding (40–42). Our lab described how injury leads to upregulation of DRG cell body and axonal localized UPR elements including GRP78/BiP and CHOP, which are retrogradely transported to the soma of injured DRG neurons (7). However, the need for a coordinated and controlled UPR/ER stress response for axon regeneration had not been proven. With a sciatic nerve injury model, Onate et al (8) found that ablation of the ER stress regulator XBP1, but not ATF4, delayed motor recovery, decreased macrophage recruitment and reduced myelin removal and axonal regeneration. Conversely, they found that transgenic mice overexpressing XBP1 have enhanced regenerative capacity after nerve crush injuries. These data provide evidence that certain aspects of the UPR are necessary for the injury/cell body response of sensory neurons. Our findings with respect to Luman support the theory that the Luman may serve to mitigate ER stress. Whether expression of UPR markers undergo a parallel biphasic response to injury as Luman is the focus of current investigation.

Prior to injury, Luman is expressed predominantly in small- to medium-size neurons associated with nociceptive function, reported here and previously (43). The greatest initial rise in Luman expression post-injury 2-day post-axotomy occurs in this subpopulation of injured neurons (Figs 3 and 4). This subpopulation is highly metabolically active with regards to glucose metabolism (44) and growth potential, having high baseline expression of growth-associated proteins (45). The plasticity-associated protein brain-derived neurotrophic factor (BDNF) is also highly expressed in this subpopulation in the intact state. Like Luman, its expression increases early post-injury in this subpopulation, where we have shown it plays a critical role in the induction of the regeneration response in sensory neurons (34, 46). It is not surprising that Luman is expressed at high levels early after injury as it too has been linked to early axon outgrowth (7, 12) and evidence suggests that small- and medium-sized sensory neurons are more primed for growth compared to larger neurons (47). The initial rise in Luman in this subpopulation also infers that they likely face a greater amount of ER stress as they transition more rapidly to a growth state. We also identified that the highest intrinsic capacity of the injured neuron for axonal growth appears to be shortly after injury (2 days), supporting that repair strategies may be bolstered if done at this early timepoint.

Prolonged peripheral nerve injury has been shown to effect a phenotypic switch in DRG sensory neurons. For example, the initial increases in BDNF are most evident in small- to medium-size neurons early after injury. BDNF expression then declines in this subpopulation and by 1-week post-injury there is increased expression in large-size neurons (46, 48, 49). The temporal biphasic response to injury with respect to Luman expression, peaking 2 days after injury in the small- to medium-size neurons, then falling across all size ranges by 4 days and rising again in all size ranges by 1 week, supports the existence of distinct phases to the injury response. Indeed, there are multiple transcriptional phases that take place as a

FIGURE 6. Continued
controls (n = 3 animals analyzed/timepoint). Scale bar = 100 μm. Graph insert: qRT-PCR analysis of Luman mRNA from injured DRG and contralateral uninjured DRG relative to naïve controls (n = 3 experimental replicates/timepoint). Note: The rise in transcript levels observed in injured DRG reached significance at 2-day post-injury and remained unchanged ($p < 0.03$). The relative increase in Luman mRNA levels in DRG neuron cell bodies ipsilateral to injury is also observed using in situ hybridization. No significant change in Luman mRNA levels was observed in DRG contralateral to injury using either approach.

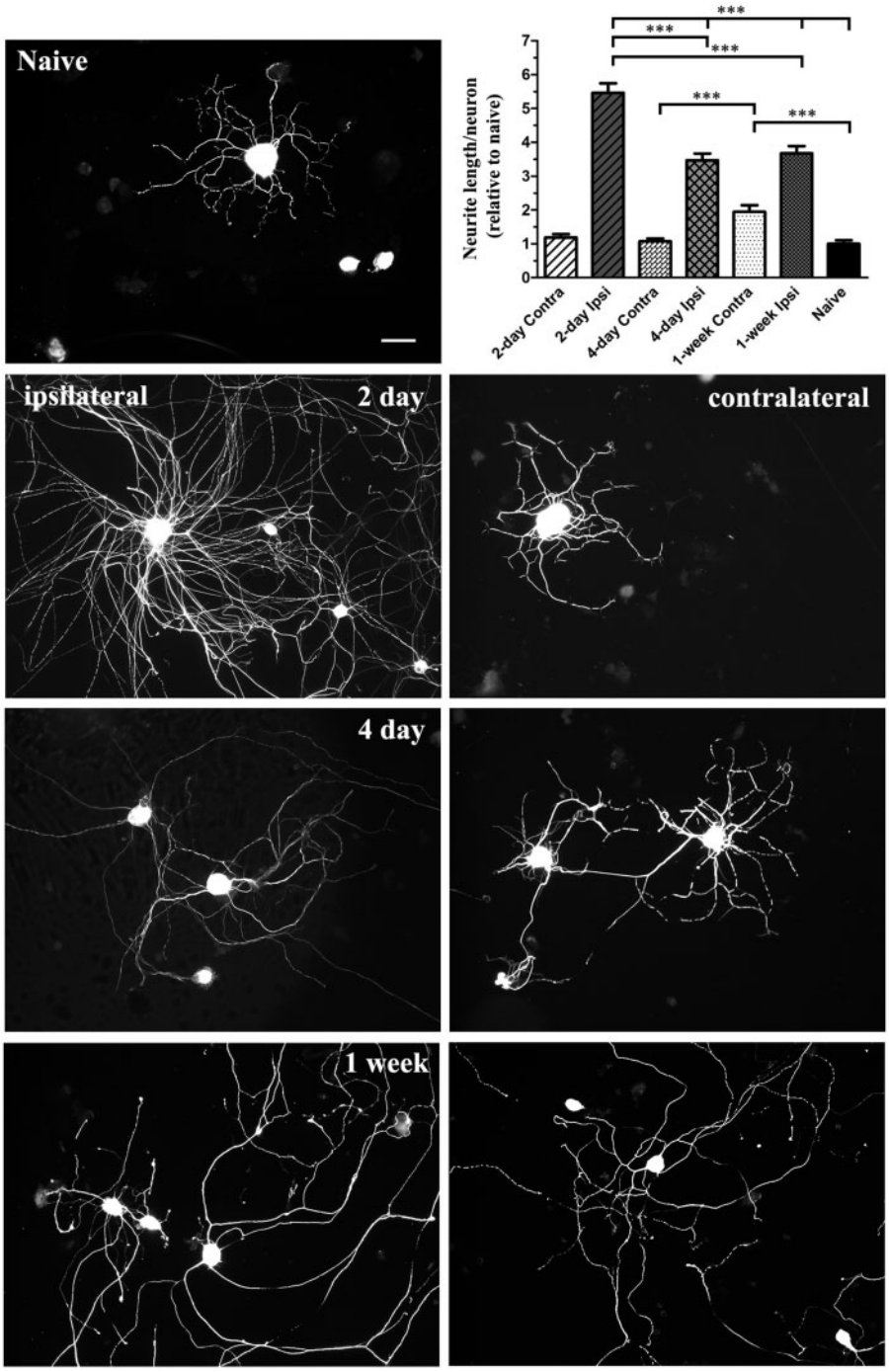

FIGURE 7. Assay reveals phasic injury-associated changes in intrinsic axonal/neurite growth capacity in injury-conditioned and uninjured contralateral sensory neurons. Fluorescence photomicrographs depicting βIII-tubulin-immunopositive staining in naïve, ipsilateral injury-conditioned (left column) and contralateral uninjured (right column) L4–L6 dorsal root ganglion (DRG) neurons assayed for 24 hours on laminin and poly-L-lysine coated coverslips (timepoints as indicated). Scale bar = 50 μm. Graph insert (upper right) summarizing the mean (± SEM) total axon/neurite length per neuron relative to naïve from DRG ipsilateral or contralateral to injury at timepoints as indicated (n = 200–250 neurons analyzed/timepoint from 3 separate time courses). Note: intrinsic axon/neurite outgrowth capacity increases significantly (***$p < 0.001$) following injury with peak outgrowth observed in the 2-day injury group, which qualitatively exhibits both highly arborized and elongating forms of growth, versus the 4- and 7-day injury-conditioned neurons that qualitatively exhibit predominantly the elongating form of outgrowth. In the uninjured contralateral DRG neurons, significantly increased outgrowth is only observed in the contralateral to 1-week injury group and is qualitatively of the predominantly elongating form normally associated with injury-conditioned neurons.

homeostatic DRG neuron transitions to a regenerating one (50, 51). A recent study used cDNA microarray analysis to identify the different genes expressed by DRG neurons after sciatic nerve transection overtime (23). The expressed genes belong to multiple biological processing including the detection of stimulus, signal transduction, the response to stimulus, transcription mechanics, regeneration and growth, and various others. Interestingly, they found 3 distinct transcriptional phases throughout the injury time course where the upregulation or downregulation of genes serve a common purpose. These phases included: (i) the "stress-response" phase occurring at 0.5–6 hours post-injury, which was enriched with transcription events associated with detection of stimulus and signal transduction; (ii) the "pre-regeneration phase" at approximately 9 hours to 1 day corresponded to increased regulation of DNA replication and transcription and elevated molecular functions such as "transcription factor activity"; and (iii) a "regeneration phase" beginning at 4 days showed processes related to cell proliferation, growth, and growth factor activity. The groups' molecular function analysis showed a multiphasic trend with regards to transcription factor activity post-injury with a peak during the early phase (approximately 9-hour mark) and a marked decrease at the 4-day timepoint, the transition point from a "pre-regeneration" to a regeneration phase, and a gradual increase thereafter. This trend shows a close similarity to the finding with Luman as levels are significantly shutdown in both the ipsilateral and contralateral neurons at 4 days, then increase at the 1-week point.

What drives the dramatic downregulation in Luman expression at 4 days, especially in light of no discernible decline in mRNA expression, is not yet known. However, the Luman protein transactivation domain is very unstable upon cleavage, being rapidly degraded and usually only readily visualized in vitro with the use of protease inhibitors (14). Recently, the Jun activation domain-binding protein 1 (JAB1) was identified as a specific inhibitor of Luman. It acts by increasing Luamn's degradation (52), which builds an argument that the primary regulatory mechanism for Luman protein expression occurs at the protein level. Thus, at 4 days, the possibility exists that there is elevation of its degradation, a cellular event that needs to be examined. Regardless, the temporal pattern of Luman immunoreactivity in injured neurons appears to coordinate nicely with the transition timepoints of the identified transcriptional phases.

Implication of the Contralateral Effect

An interesting aspect of this study was the effect of unilateral axotomy on neuronal Luman expression in uninjured contralateral DRG. Contralateral neurons showed a similar biphasic, but less robust response and did not have the dramatic increase in neuronal Luman expression observed in DRG ipsilateral to the 2-day injury. Few connections exist between neurons that innervate opposite sides of the body; however, a collection of clinical evidence confirms contralateral deficits in patients with 1-sided injuries (53, 54). The bilateral impact of nerve injury has been reported in a number of animal models where sensory, sympathetic, or motoneurons opposite to the lesion site differ morphologically and/or biochemically from naïve controls (55). In addition to these changes, neurons of intact DRG contralateral or segmentally adjacent to the injured ganglia have altered nerve sprouting in unaffected limb areas (56–58). Contralateral DRG neurons may have altered neurotrophin signaling, as unilateral sciatic nerve injury causes increased p75 receptor expression in perineuronal glial cells in contralateral DRG (59). In general, these observations are considered a result of a neural mechanism with a propagating signal through the spinal cord, and not due to a systemic effect.

The contralateral alterations in Luman expression were also biphasic, with a significant drop in expression at the 4-day timepoint, suggesting that these phases have distinct humeral signatures. However, the initial early 1-hour response was more robust in contralateral ganglia implying that disconnection from target ipsilateral to injury may serve to dampen the initial stress response associated with axotomy. Notably, the changes in contralateral Luman expression and localization were not reflected in corresponding changes in transcript levels, which remained relatively stable over the time course, unlike the observed ipsilateral changes. Any change in this regulator of the UPR would imply that the contralateral DRG neurons are experiencing varying degrees of ER stress, although this needs to be determined. As explained above, the 4-day timepoint corresponds to a significant transition point in the injury response of sensory neurons when transcription factor activity and transcriptional activation is depressed. Thus, presumably there would also be less of a need for a coordinated UPR.

The increased Luman expression and significantly increased intrinsic axon growth competence that we observed in neurons contralateral to 1-week injury support previous work by the Ryoke et al (60) showing that a prior lesion can serve to condition contralateral DRG to express higher levels of protective and growth-promoting compounds, and to regenerate more robustly when subsequently injured (61). Interestingly, we found the mode of axon growth to be predominantly of the elongating form typically associated with the 1-week injury-conditioned neurons (31), as opposed to the highly arborized outgrowth we observed for contralateral neurons at the 2 earlier timepoints, which did not differ from that observed for naïve neurons and is in agreement with that which we previously reported for neurons contralateral to 1-day injury (12). Whether, the increased levels of Luman always serve to advantage contralateral neurons is not known. The reality of contralateral and humeral effects of nerve injury illustrates the importance of using naïve animals and not contralateral uninjured tissue as controls.

Humoral/Systemic Influences in Injury Responses

Systemic inflammatory responses are well-defined clinical entities where a severe insult to the organism results in a systemic cascade of inflammatory mediators causing hemodynamic instability, end organ damage, and potentially multisystem organ failure (62). Spinal cord injury (SCI) is 1 such case where evidence suggests pathological connections emanating from the injured spinal cord result in a profound and sustained intraspinal and systemic inflammatory response with increased circulation of immune cells and proinflammatory

mediators resulting in distal end organ dysfunction (reviewed in [63]). Following transection of a peripheral nerve, the severed distal segment undergoes Wallerian degeneration where an inflammatory driven process leads to macrophage invasion and clearance of the damaged axons and associated glia (64). While release of breakdown products and inflammatory markers from the lesion site into the circulation is likely to occur, there is a paucity of studies investigating the impact of peripheral nerve injury on systemic inflammatory states. It is unknown whether these signals exist at a level to potentially contribute to a contralateral affect.

There is also dysregulation of the neuroendocrine system in SCI subjects with increased activation of the hypothalamic-pituitary-adrenal (HPA) axis, a potent endocrine regulator of stress and inflammation. Elevated levels of glucocorticoids are the end result of this dysregulation (65). Circulating levels of endogenous corticosterone (rodents) and cortisol (humans) increase after SCI (66, 67), undoubtedly affecting multiple glucocorticoid receptor (GR)-regulated cellular functions; however, specifics of GR signaling are not well defined in the context of nervous system injury. The impact of peripheral nerve damage on the HPA axis is also not well understood but DRG neurons express GRs, while steroid or HPA axis manipulation has been shown to alter DRG neuron phenotypic expression patterns (68–70). Thus, it is plausible to consider glucocorticoids as a potential contributor to either bilateral, contralateral, or systemic sensory nerve injury changes but the response of the HPA in the injured state needs to be characterized. Interestingly, Luman has recently been identified as a key regulator of glucocorticoid-mediated stress responses through its ability to modulate GR expression and activity (70) by binding to the GR (71). Whether this factors into the response to peripheral nerve injury remains to be determined.

Altered neurotrophin signaling has also been a suspected contributor to the contralateral effect. Most recently, Shakhbazau et al (32) discovered that unilateral sciatic nerve transection resulted in elevation of NGF and NT3, but not glial-derived neurotrophic factor or BDNF, in the uninjured contralateral nerve. This evidence suggests that unilateral injury can regulate systemic neurotrophin levels and therefore enhance neurotrophin signaling in uninjured DRG neurons. However, the link between systemic implications of PNS pathologies and observed contralateral responses must be better elucidated before they can be attributed to changes in contralateral neurons.

Conclusion

Peripheral neurons do grow axons after nerve injury, but repair is often slow and functional recovery is poor. Evidence supports the necessity of a coordinated UPR and the induction of specific UPR regulators for optimal regeneration to occur. While we had previously identified axonal Luman as a key sensor of injury, regulating the UPR and cholesterol biosynthesis in DRG neurons critically linked to acute axonal growth capacity, we now show Luman is also part of the injury-associated cell body response. Its upregulation and nuclear localization coordinates with recently identified timepoints of increased transcriptional activity in injured neurons. Elucidating how Luman/CREB3 is altered spatially and temporally and how this correlates with changes in intrinsic axon growth capacity at the different timepoints examined has the potential to inform when therapeutic intervention or repair may be most effective.

REFERENCES

1. Redshaw JD, Bisby MA. Proteins of fast axonal transport in regenerating rat sciatic sensory axons: A conditioning lesion does not amplify the characteristic response to axotomy. Exp Neurol 1987;98:212–21
2. Vance JE, Campenot RB, Vance DE. The synthesis and transport of lipids for axonal growth and nerve regeneration. Biochim Biophys Acta 2000;1486:84–96
3. Galbraith JA, Gallant PE. Axonal transport of tubulin and actin. J Neurocytol 2000;29:889–911
4. Koenig E, Martin R, Titmus M, et al. Cryptic peripheral ribosomal domains distributed intermittently along mammalian myelinated axons. J Neurosci 2000;20:8390–400
5. Saxena S, Cabuy E, Caroni P. A role for motoneuron subtype-selective ER stress in disease manifestations of FALS mice. Nat Neurosci 2009;2:627–36
6. Schroder M, Kaufman RJ. ER stress and the unfolded protein response. Mutat Res 2005;569:29–63
7. Ying Z, Zhai R, McLean NA, et al. The unfolded protein response and cholesterol biosynthesis link Luman/CREB3 to regenerative axon growth in sensory neurons. J Neurosci 2015;35:14557–70
8. Onate M, Catenaccio A, Martinez G, et al. Activation of the unfolded protein response promotes axonal regeneration after peripheral nerve injury. Sci Rep 2016;6:21709
9. Naidoo N. The endoplasmic reticulum stress response and aging. Rev Neurosci 2009;20:23–37
10. Inceoglu B, Bettaieb A, Trindade da Silva CA, et al. Endoplasmic reticulum stress in the peripheral nervous system is a significant driver of neuropathic pain. Proc Natl Acad Sci USA 2015;112:9082–7
11. Hetz C, Saxena S. ER stress and the unfolded protein response in neurodegeneration. Nat Rev Neurol 2017;13:477–91
12. Ying Z, Misra V, Verge VM, Sensing nerve injury at the axonal ER: Activated Luman/CREB3 serves as a novel axonally synthesized retrograde regeneration signal. Proc Natl Acad Sci USA 2014;111:16142–7
13. Lu R, Yang P, Padmakumar S, et al. The herpesvirus transactivator VP16 mimics a human basic domain leucine zipper protein, luman, in its interaction with HCF. J Virol 1998;72:6291–7
14. Lu R, Yang P, O'Hare P, et al. Luman, a new member of the CREB/ATF family, binds to herpes simplex virus VP16-associated host cellular factor. Mol Cell Biol 1997;17:5117–26
15. Freiman RN, Herr W. Viral mimicry: Common mode of association with HCF by VP16 and the cellular protein LZIP. Genes Dev 1997;11:3122–7
16. Lu R, Misra V. Potential role for luman, the cellular homologue of herpes simplex virus VP16 (alpha gene trans-inducing factor), in herpesvirus latency. J Virol 2000;74:934–43
17. Haze K, Yoshida H, Yanagi H, et al. Mammalian transcription factor ATF6 is synthesized as a transmembrane protein and activated by proteolysis in response to endoplasmic reticulum stress. Mol Biol Cell 1999;10:3787–99
18. Raggo C, Rapin N, Stirling J, et al. Luman, the cellular counterpart of herpes simplex virus VP16, is processed by regulated intramembrane proteolysis. Mol Cell Biol 2002;22:5639–49
19. Misra V, Rapin N, Akhova O, et al. Zhangfei is a potent and specific inhibitor of the host cell factor-binding transcription factor Luman. J Biol Chem 2005;280:15257–66
20. Liang G, Audas TE, Li Y, et al. Luman/CREB3 induces transcription of the endoplasmic reticulum (ER) stress response protein Herp through an ER stress response element. Mol Cell Biol 2006;26:7999–8010
21. Kim TY, Kim E, Yoon SE, et al. Herp enhances ER-associated protein degradation by recruiting ubiquilins. Biochem Biophys Res Commun 2008;369:741–6
22. DenBoer LM, Hardy-Smith PW, Hogan MR, et al. Luman is capable of binding and activating transcription from the unfolded protein response element. Biochem Biophys Res Commun 2005;331:113–9

23. Li S, Xue C, Yuan Y, et al. The transcriptional landscape of dorsal root ganglia after sciatic nerve transection. Sci Rep 2015;5:16888
24. Ying Z, Zhang R, Verge VM, et al. Cloning and characterization of rat Luman/CREB3, a transcription factor highly expressed in nervous system tissue. J Mol Neurosci 2015;55:347–54
25. Gambarotta G, Ronchi G, Friard O, et al. Identification and validation of suitable housekeeping genes for normalizing quantitative real-time PCR assays in injured peripheral nerves. PLoS One 2014;9:e105601
26. Tsujino H, Kondo E, Fukuoka T, et al. Activating transcription factor 3 (ATF3) induction by axotomy in sensory and motoneurons: A novel neuronal marker of nerve injury. Mol Cell Neurosci 2000;15:170–82
27. Seijffers R, Allchorne AJ, Woolf CJ. The transcription factor ATF-3 promotes neurite outgrowth. Mol Cell Neurosci 2006;32:143–54
28. Verge VM, Merlio JP, Grondin J, et al. Colocalization of NGF binding sites, trk mRNA, and low-affinity NGF receptor mRNA in primary sensory neurons: Responses to injury and infusion of NGF. J Neurosci 1992; 12:4011–22
29. Verge VM, Richardson PM, Benoit R, et al. Histochemical characterization of sensory neurons with high-affinity receptors for nerve growth factor. J Neurocytol 1989;18:583–91
30. Kleinschnitz C, Brinkhoff J, Sommer C, et al. Contralateral cytokine gene induction after peripheral nerve lesions: Dependence on the mode of injury and NMDA receptor signaling. Brain Res Mol Brain Res 2005; 136:23–8
31. Miao P, Madec K, Gong Y, et al. Axotomy-induced up-regulation of tumor necrosis factor-alpha in the dorsal root ganglia. Neurol Res 2008;30: 623–31
32. Shakhbazau A, Martinez JA, Xu QG, et al. Evidence for a systemic regulation of neurotrophin synthesis in response to peripheral nerve injury. J Neurochem 2012;122:501–11
33. Smith DS, Skene JH. A transcription-dependent switch controls competence of adult neurons for distinct modes of axon growth. J Neurosci 1997;17:646–58
34. Geremia NM, Pettersson LM, Hasmatali JC, et al. Endogenous BDNF regulates induction of intrinsic neuronal growth programs in injured sensory neurons. Exp Neurol 2010;223:128–42
35. Audas TE, Li Y, Liang G, et al. A novel protein, Luman/CREB3 recruitment factor, inhibits Luman activation of the unfolded protein response. Mol Cell Biol 2008;28:3952–66
36. Watson WE. Cellular responses to axotomy and to related procedures. Br Med Bull 1974;30:112–5
37. Raivich G, Bohatschek M, Da Costa C, et al. The AP-1 transcription factor c-Jun is required for efficient axonal regeneration. Neuron 2004;43: 57–67
38. Bomze HM, Bulsara KR, Iskandar BJ, et al. Spinal axon regeneration evoked by replacing two growth cone proteins in adult neurons. Nat Neurosci 2001;4:38–43
39. Penas C, Font-Nieves M, Fores J, et al. Autophagy, and BiP level decrease are early key events in retrograde degeneration of motoneurons. Cell Death Differ 2011;18:1617–27
40. Noel F, Frost WN, Tian LM, et al. Recovery of tail-elicited siphon-withdrawal reflex following unilateral axonal injury is associated with ipsi- and contralateral changes in gene expression in *Aplysia californica*. J Neurosci 1995;15:6926–38
41. Willis D, Li KW, Zheng JQ, et al. Differential transport and local translation of cytoskeletal, injury-response, and neurodegeneration protein mRNAs in axons. J Neurosci 2005;25:778–91
42. Castillo V, Onate M, Woehlbier U, et al. Functional role of the disulfide isomerase ERp57 in axonal regeneration. PLoS One 2015;10:e0136620
43. Lindsay RM. Role of neurotrophins and trk receptors in the development and maintenance of sensory neurons: An overview. Philos Trans R Soc Lond B Biol Sci 1996;351:365–73
44. Gardiner NJ, Wang Z, Luke C, et al. Expression of hexokinase isoforms in the dorsal root ganglion of the adult rat and effect of experimental diabetes. Brain Res 2007;1175:143–54
45. Verge VM, Tetzlaff W, Richardson PM, et al. Correlation between GAP43 and nerve growth factor receptors in rat sensory neurons. J Neurosci 1990;10:926–34
46. Karchewski LA, Gratto KA, Wetmore C, et al. Dynamic patterns of BDNF expression in injured sensory neurons: Differential modulation by NGF and NT-3. Eur J Neurosci 2002;16:1449–62
47. Andersen LB, Schreyer DJ. Constitutive expression of GAP-43 correlates with rapid, but not slow regrowth of injured dorsal root axons in the adult rat. Exp Neurol 1999;155:157–64
48. Cho HJ, Kim JK, Park HC, et al. Changes in brain-derived neurotrophic factor immunoreactivity in rat dorsal root ganglia, spinal cord, and gracile nuclei following cut or crush injuries. Exp Neurol 1998;154:224–30
49. Tonra JR, Curtis R, Wong V, et al. Axotomy upregulates the anterograde transport and expression of brain-derived neurotrophic factor by sensory neurons. J Neurosci 1998;18:4374–83
50. Costigan M, Befort K, Karchewski L, et al. Replicate high-density rat genome oligonucleotide microarrays reveal hundreds of regulated genes in the dorsal root ganglion after peripheral nerve injury. BMC Neurosci 2002;3:16
51. Christie KJ, Webber CA, Martinez JA, et al. PTEN inhibition to facilitate intrinsic regenerative outgrowth of adult peripheral axons. J Neurosci 2010;30:9306–15
52. DenBoer LM, Iyer A, McCluggage AR, et al. JAB1/CSN5 inhibits the activity of Luman/CREB3 by promoting its degradation. Biochim Biophys Acta 2013;1829:921–9
53. Kozin F, Genant HK, Bekerman C, et al. The reflex sympathetic dystrophy syndrome. II. Roentgenographic and scintigraphic evidence of bilaterality and of periarticular accentuation. Am J Med 1976;60:332–8
54. Oaklander AL, Romans K, Horasek S, et al. Unilateral postherpetic neuralgia is associated with bilateral sensory neuron damage. Ann Neurol 1998;44:789–95
55. Koltzenburg M, Wall PD, McMahon SB. Does the right side know what the left is doing? Trends Neurosci 1999;22:122–7
56. Devor M, Schonfeld D, Seltzer Z, et al. Two modes of cutaneous reinnervation following peripheral nerve injury. J Comp Neurol 1979;185: 211–20
57. Navarro X, Verdú E, Wendelschafer-Crabb G, et al. Immunohistochemical study of skin reinnervation by regenerative axons. J Comp Neurol 1997;380:164–74
58. Oaklander AL, Brown JM. Unilateral nerve injury produces bilateral loss of distal innervation. Ann Neurol 2004;55:639–44
59. Zhou XF, Rush RA, McLachlan EM. Differential expression of the p75 nerve growth factor receptor in glia and neurons of the rat dorsal root ganglia after peripheral nerve transection. J Neurosci 1996;16:2901–11
60. Ryoke K, Ochi M, Iwata A, et al. A conditioning lesion promotes in vivo nerve regeneration in the contralateral sciatic nerve of rats. Biochem Biophys Res Commun 2000;267:715–8
61. Senger JB, Verge VM, Chan KM, et al. The nerve conditioning lesion: A strategy to enhance nerve regeneration. Ann Neurol 2018;83:691–702
62. Balk RA. Systemic inflammatory response syndrome (SIRS): Where did it come from and is it still relevant today? Virulence 2014;5:20–6
63. Sun X, Jones ZB, Chen XM, et al. Multiple organ dysfunction and systemic inflammation after spinal cord injury: A complex relationship. J Neuroinflamm 2016;13:260
64. Rotshenker S. Wallerian degeneration: The innate-immune response to traumatic nerve injury. J Neuroinflamm 2011;8:109
65. Lerch JK, Puga DA, Bloom O, et al. Glucocorticoids and macrophage migration inhibitory factor (MIF) are neuroendocrine modulators of inflammation and neuropathic pain after spinal cord injury. Semin Immunol 2014;26:409–14
66. Cruse JM, Keith JC, Bryant ML, Jr, et al. Immune system neuroendocrine dysregulation in spinal cord injury. Immunol Res 1996;15:306–14.
67. Lucin KM, Sanders VM, Jones TB, et al. Impaired antibody synthesis after spinal cord injury is level dependent and is due to sympathetic nervous system dysregulation. Exp Neurol 2007;207:75–84
68. Smith GD, Seckl JR, Sheward WJ, et al. Effect of adrenalectomy and dexamethasone on neuropeptide content of dorsal root ganglia in the rat. Brain Res 1991;564:27–30
69. Covenas R, DeLeon M, Chadi G, et al. Adrenalectomy increases the number of substance P and somatostatin immunoreactive nerve cells in the rat lumbar dorsal root ganglia. Brain Res 1994;640:352–6
70. Penney J, Mendell A, Zeng M, et al. LUMAN/CREB3 is a key regulator of glucocorticoid-mediated stress responses. Mol Cell Endocrinol 2017; 439:95–104
71. Penney J, Taylor T, MacLusky N, et al. LUMAN/CREB3 plays a dual role in stress responses as a cofactor of the glucocorticoid receptor and a regulator of secretion. Front Mol Neurosci 2018;11:352